Received: 10 September 2019 | Revised: 20 November 2019 | Accepted: 23 November 2019

DOI: 10.1002/mrm.28128

FULL PAPER

Magnetic Resonance in Medicine

Reduction of vibration-induced signal loss by matching mechanical vibrational states: Application in high *b*-value diffusion-weighted MRS

Dominik Weidlich[1] | **Mark Zamskiy**[1] | **Marcus Maeder**[2] | **Stefan Ruschke**[1] | **Steffen Marburg**[2] | **Dimitrios C. Karampinos**[1]

[1]Department of Diagnostic and Interventional Radiology, School of Medicine, Technical University of Munich, Munich, Germany

[2]Chair of Vibroacoustics of Vehicles and Machines, Technical University of Munich, Garching, Germany

Correspondence
Dominik Weidlich, Department of Diagnostic and Interventional Radiology, Klinikum rechts der Isar, School of Medicine, Technical University of Munich, Ismaninger St. 22, 81675 Munich, Germany.
Email: dominik.weidlich@tum.de

Funding information
Supported by the European Research Council, grant agreement 677661, ProFatMRI; and Philips Healthcare

Purpose: Diffusion encoding gradients are known to yield vibrations of the typical clinical MR scanner hardware with a frequency of 20 to 30 Hz, which may lead to signal loss in diffusion-weighted MR measurements. This work proposes to mitigate vibration-induced signal loss by introducing a vibration-matching gradient (VMG) to match vibrational states during the 2 diffusion gradient pulses.

Theory and Methods: A theoretical description of displacements induced by gradient switching was introduced and modeled by a 2-mass-spring-damper system. An additional preceding VMG mimicking timing and properties of the diffusion encoding gradients was added to a high *b*-value diffusion-weighted MR spectroscopy sequence. Laser interferometry was employed to measure 3D displacements of a phantom surface. Lipid ADC was assessed in water–fat phantoms and in vivo in the tibial bone marrow of 3 volunteers.

Results: The modeling and the laser interferometer measurements revealed that the displacement curves are more similar during the 2 diffusion gradients with the VMG compared to the standard sequence, resulting in less signal loss of the diffusion-weighted signal. Phantom results showed lipid ADC overestimation up to 119% with the standard sequence and an error of 5.5% with the VMG. An 18% to 35% lower coefficient of variation was obtained for in vivo lipid ADC measurement when employing the VMG.

Conclusion: The application of the VMG reduces the signal loss introduced by hardware vibrations in a high *b*-value diffusion-weighted MRS sequence in phantoms and in vivo. Reference measurements based on laser interferometry and mechanical modelling confirmed the findings.

KEYWORDS
artifact reduction, diffusion weighting, high *b*-value, mechanical vibrations, scanner table vibrations

1 | INTRODUCTION

Diffusion-weighted (DW) MR is a powerful tool for the noninvasive assessment of tissue microstructure and is widely applied in the clinical routine as well as in research applications.[1] Sensitizing the MR measurement to diffusion requires strong diffusion-encoding gradients, bringing up technical challenges related to increased sensitivity to motion effects,[2] eddy currents,[3] and scanner table vibrations.[4] Specifically, diffusion-encoding gradients were shown to yield vibrations of the scanner hardware (e.g., scanner table vibrations during diffusion tensor imaging with a frequency of 20-30 Hz and amplitudes up to 100 μm).[5] The observed vibrations were so strong that even elastography experiments utilizing the table vibrations as the main source of mechanical actuation have been proposed.[6] The observed influences of additional vibration-induced motion include reports of signal loss in brain DW images[7,8] and reports of increased lipid ADC measures in subcutaneous fat in regions close to the scanner table.[4]

Multiple research applications require particularly high *b*-values diffusion measurements, including high-resolution diffusion tensor imaging of the brain[9] or the assessment of fat microstructure with diffusion MRI.[10-12] Specifically, measuring the diffusion properties of lipids has been proven to be challenging because fat has a diffusion coefficient approximately 2 orders of magnitude lower than water due to the large molecular size.[4,13] The assessment of fat microstructure is important in the study of adipose tissue and ectopic lipids in both healthy subjects and subjects affected by metabolic dysfunction across organs and tissues. The quantification of lipid droplet size with DW MR is of great interest in skeletal muscle research,[14] in metabolic research differentiating brown and white adipocytes,[15] and in bone marrow research aiming at the quantification of bone marrow adipocyte size.[16]

Measuring high-resolution diffusion features or diffusion restriction effects requires the acquisition of an artifact-free DW signal while employing high *b*-values. Given that the gradient strength of clinical MR scanners is limited, high *b*-values are typically associated with long diffusion gradients at the maximum allowed gradient amplitude. Scanner table vibration effects induced by the long and strong diffusion gradients can become significant at certain frequencies of the scanner hardware mechanical system.[5]

Any motion during the diffusion sensitizing period induces an additional accumulated phase and eventually leads to signal cancellations due to intravoxel dephasing.[17] The amount of the intravoxel dephasing by motion scales at a first approximation with the first gradient moment. Tissue displacements induced by mechanical vibrations introduce such intravoxel dephasing. The amount of intravoxel dephasing increases in the presence of strong and long diffusion encoding gradients. Therefore, tissue displacements induced by mechanical vibrations at high *b*-value scanning compromise the reliability of the measured DW signal for any subsequent analysis aiming at the extraction of quantitative diffusion parameters.

The present work proposes the application of an additional gradient before the actual diffusion sensitizing period to mitigate signal loss induced by scanner table vibrations. The benefits of the proposed approach are shown by modeling a simplified mechanical model and the quantification of the scanner table displacements with and without the additional gradient by doppler laser interferometry. Afterward, the approach is tested measuring lipid ADC with a DW MRS sequence in water–fat (WF) phantoms and in vivo in the tibial bone marrow of healthy volunteers.

2 | THEORY

2.1 | Mechanical description

Modulation of magnetic field gradients is an essential element of most MR pulse sequences. Alterations of the magnetic gradient strength or polarity are achieved by changing the current in the respective gradient coil. Time-varying currents in the strong main magnetic field result in Lorentz forces on the gradient coil. The mechanical vibrations of the MR hardware components are eventually caused by the impact of the gradient coils on the mounting during the MR experiment.[18] The Lorentz forces on the gradient coils also induce vibrations of the MR scanner table that are subsequently transferred to the object that is examined. The propagation of the vibrations within the object and the damping of the displacement amplitude are dependent on the mechanical properties of the system. Consequently, the forces on the MR gradient hardware can induce time-varying displacements within the subject or object being scanned.

However, the exact displacement pattern within the tissue might be difficult to predict. Although the vibrations do not originate from the scanner table, the observed vibrations will be referred to as scanner table vibrations.

2.2 | MR diffusion encoding

Using MR, diffusion properties can be probed using 2 diffusion encoding gradients and a time interval between these 2 diffusion encoding gradients[19] (Figure 1). The accumulated phase during the first diffusion encoding gradient (DG_1) is recovered by the accumulated phase during the second diffusion gradient (DG_2) for stationary spins. For moving spins, any phase dispersion is not recovered and consequently leads to signal loss. In the absence of any macroscopic motion or flow effects, the strength of the signal loss reflects the self-diffusion of the particles; therefore, information about the

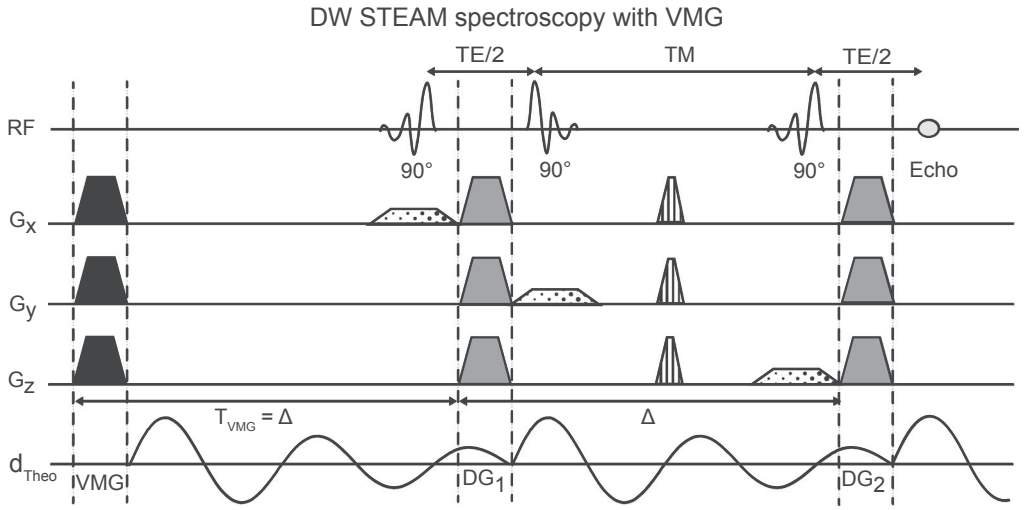

FIGURE 1 Sequence diagram of the DW-STEAM sequence with the proposed VMG (in black) and corresponding d_{Theo} induced by the strong gradient waveforms. The DW-STEAM magnetization preparation consists of 3 slice-selective 90° RF pulses and monopolar diffusion sensitizing gradients (in gray). Spoiler gradients (vertical stripes) and slice selective gradients (dots) are also shown. Both the VMG and the diffusion gradients will lead to tissue displacements. If a VMG is introduced with appropriate timing, the tissue displacement pattern is similar during DG_1 and DG_2. Δ, diffusion time; DG_1, first diffusion gradient; DG_2, second diffusion gradient; d_{Theo}, theoretical tissue displacement; DW, diffusion-weighted; TM, mixing time; T_{VMG}, timing of vibration-matching gradient; VMG, vibration-matching gradient

tissue microstructure can be extracted. Mathematically, the accumulated phase ϕ at time t for a spin located at position $\vec{r}_0$ at time $t = 0$ can be expressed as:

$$\phi\left(\vec{r}_0, t\right) = \gamma \int_0^t \vec{G}\left(t'\right) \cdot \vec{r}\left(\vec{r}_0, t'\right) dt', \tag{1}$$

where γ is the gyromagnetic ratio; $\vec{G}$ is the magnetic field gradient; and $\vec{r}\left(\vec{r}_0, t'\right)$ is the location at time t for a spin located at position $\vec{r}_0$ at time $t = 0$. The total signal S acquired from a defined volume of spins can be expressed as:

$$S(t) = S_0 \int e^{-i\phi(\vec{r}_0, t)} d\vec{r}_0. \tag{2}$$

Any additional accumulated phase that is not due to diffusion can lead to additional signal decay and consequently results in quantification errors.

2.3 | MR diffusion encoding in the presence of vibrations

The bottom row of Figure 1 depicts a schematic view of the displacements induced by DG_1 that will be present during the presence of DG_2. Assuming a simple diffusion encoding scheme with a time separation and a refocusing element between the 2 diffusion weighting gradients and assuming rectangular gradients, the phase at the end of the DW can be expressed as:

$$\phi\left(\vec{r}_0, \Delta + \delta\right) = \gamma G \left[\int_0^{\delta} \vec{r}\left(\vec{r}_0, t'\right) dt' - \int_{\Delta}^{\Delta+\delta} \vec{r}\left(\vec{r}_0, t'\right) dt'\right]. \tag{3}$$

Here, δ is the length of the DW gradient, and Δ is the diffusion time. When the spins are affected only by the motion due to vibrations (assuming no diffusion or flow effects), only the displacements from the equilibrium position ($\vec{d}$) can be considered. The second integral can be simplified by a coordinate transformation:

$$\begin{aligned}\phi\left(\vec{r}_0, \Delta + \delta\right) &= \gamma G \left[\int_0^{\delta} \vec{d}\left(\vec{r}_0, t'\right) dt' - \int_0^{\delta} \vec{d}\left(\vec{r}_0, t' + \Delta\right) dt'\right] \\ &= \gamma G \int_0^{\delta} \left[\vec{d}\left(\vec{r}_0, t'\right) - \vec{d}\left(\vec{r}_0, t' + \Delta\right)\right] dt'\end{aligned} \tag{4}$$

$$S = S_0 \int e^{-i\phi(\vec{r}_0, \Delta+\delta)} d\vec{r}_0 = S_0 \int e^{-i\gamma G \int_0^{\delta} \left[\vec{d}(\vec{r}_0, t') - \vec{d}(\vec{r}_0, t'+\Delta)\right] dt'} d\vec{r}_0. \tag{5}$$

Equation 5 shows that signal loss due to vibrational displacements can occur when the displacements during the 2 diffusion gradient durations (DG_1 und DG_2) differ. Larger voxel sizes and stronger first gradient moments amplify this signal loss.[17] To minimize the phase dispersion within a voxel, the following condition should be fulfilled for all spins:

$$\vec{d}\left(\vec{r}_0, t\right) = \vec{d}\left(\vec{r}_0, t + \Delta\right) \quad \text{for } 0 < t < \delta. \tag{6}$$

This condition is not fulfilled in a standard DW sequence. DG_1 will introduce tissue displacements that in general are

different between DG_2 and DG_1. To match tissue displacements between DG_1 and DG_2 and mitigate signal loss, an additional gradient can be introduced to induce vibrations during DG_1 similar to the vibrations induced by the first diffusion gradient during DG_2. The additional gradient replicating the vibrational patterns is called vibration-matching gradient (VMG).

If the VMG is placed before DG_1 with appropriate timing, the tissue displacement pattern can become similar during both diffusion encoding gradients. The introduction of the VMG is shown in Figure 1 (see upper row). The VMG is applied before the RF excitation pulse of the diffusion sensitizing module and does not interfere with the transverse magnetization but solely induces a mechanical vibration state. When the time interval between the VMG and DG_1 is equal to the diffusion time, the tissue displacement caused by scanner table vibrations during the 2 diffusion gradients should be similar. Therefore, the accumulated phase during the diffusion encoding is similar, and the occurring signal loss can be mitigated. The mechanical vibrational pattern during the 2 diffusion gradients may become similar for other timings of the additional gradient. However, the exact optimal timing, which is when the time interval between the VMG and the DG_1 is not equal to the diffusion time, will depend on the frequency of the vibration, the coupling of the components, and the damping of the vibrations; thus, it is not easily predictable.

2.4 | Mechanical modeling of a 2-mass-spring-damper system

Most biological soft tissues can be modeled as viscoelastic materials.[20] The viscoelastic material model comprises of an elastic (spring-like) and viscous or damping (dashpot-like) response to an external force. Mathematical models have been developed to predict the dynamics and the response of viscoelastic materials.[21] The field of MR elastography deploys these models and tries to map tissue properties after intentionally applying a defined actuation to the investigated tissue during a special MR examination.[20] However, there are also involuntary actuations due to the MR scanner table, as described above. To illustrate the behavior of a viscoelastic material that is excited by an external force, the displacement of 2 masses that are connected in a spring-damper system was investigated in 1D. The system is decribed in Figure 2B, where the 2 masses could represent 2 isochromats within the viscoelastic material. They should be embedded in the material; therefore, both are connected to a larger pool represented as a fixed boundary. The excitation of the system by scanner table vibrations was represented by instantaneous force impulses on mass 1 whenever there was a gradient switching in the gradient pulse sequence shown in Figure 2A. A different direction of the impulse was assumed for different polarities of the gradient slope. It was assumed that there

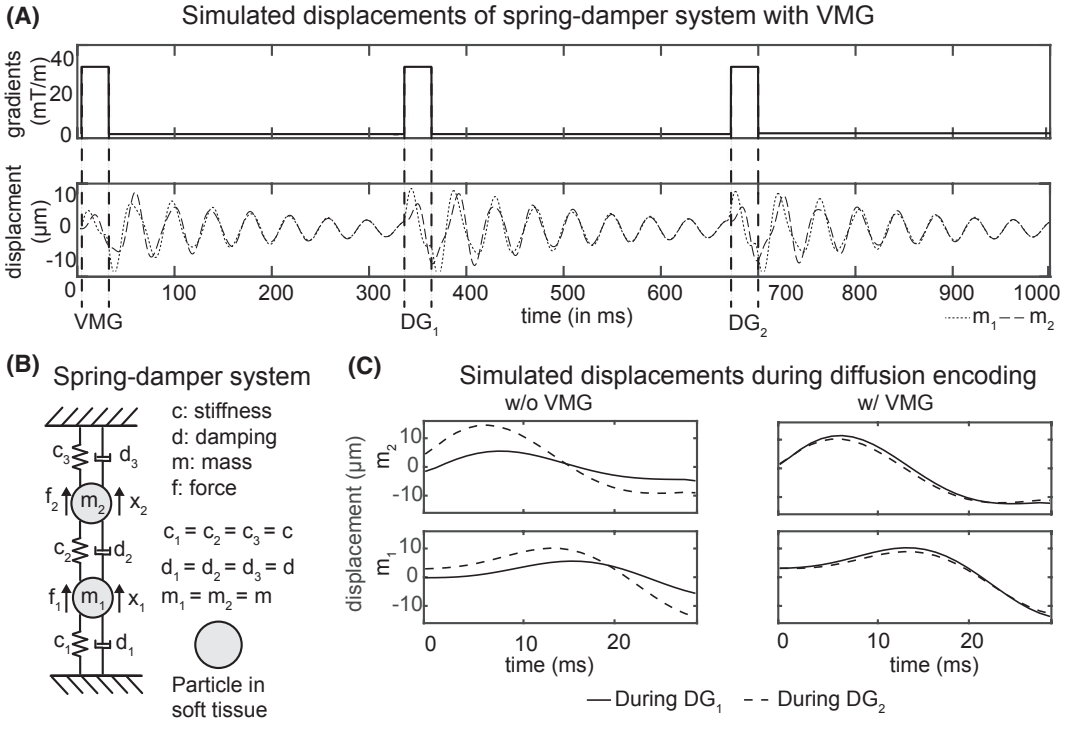

FIGURE 2 Simulated displacements during diffusion gradients assuming a 2-mass-spring-damper system (schematic B). Plot A shows the strong gradient waveforms within the pulse sequence and the corresponding simulated displacement of m_1 and m_2 when the VMG and the 2 diffusion gradients are simulated. Plot C shows the displacement of the 2 masses during DG_1 and DG_2. The displacements of the 2 masses are different without the VMG, whereas the displacements of the 2 masses are very similar with the VMG. m_1, mass 1; m_2, mass 2

was no additional force on mass 2. In the pulse sequence shown in Figure 2, the system was consequently excited by 4 Dirac impulses when no VMG was applied and was excited by 6 Dirac impulses when the VMG was employed. A mathematical derivation of equation of motion is given in the Supporting Information following Voeth et al.[22] The magnitude of the stiffness parameter of an unknown material can be estimated by the frequency of the induced vibration assuming an undamped oscillation ($c \approx 4\pi^2 m f^2$). To the best of the authors' knowledge, the mechanical parameters for adipose tissue assuming a simple 1D spring-damper system are not available in current literature.

The following parameters were assumed: mass m = 0.5 kg; stiffness c (25 Hz undamped oscillation) = 12,337 $\frac{N}{m}$; damping d was selected to be 5 $\frac{kg}{s}$ to achieve a similar damping as observed in the interferometer measurements; and the amplitude of the force impulse was selected to give a displacement amplitude equal to 10 μm. The system was solved for the gradient pulse sequence shown in Figure 2A with and without the VMG by means of numerical integration (Figure 2A).

3 | METHODS

3.1 | DW-MRS pulse sequence and spectrum analysis

To test the proposed method, the diffusion properties of lipids were measured with a bipolar DW STEAM MRS sequence (Figure 1). The sequence was based on a standard single-voxel STEAM MRS, with gradients added after the first and third RF pulse to induce diffusion-weighting. Half of the DW spectra were acquired with positive diffusion gradient polarity and half with negative. The DW spectra with opposite diffusion gradient polarity were used to estimate and compensate for eddy-current effects.[23] To mitigate the effect of vibration-induced tissue displacements on the DW signal, the VMG with identical gradient duration and amplitude properties to the diffusion sensitizing gradients was placed before the actual sequence. The data processing included zero order phasing and Gaussian apodization. The single averages were frequency-aligned, and averages with a deviation of the methylene peak amplitude of more than 2 SDs from the mean methylene peak amplitude were identified as outliers and excluded from the subsequent analysis. The remaining averages for both polarities were combined and corrected for eddy currents. Peak area quantification was performed on the real spectrum fitting 8 fat peaks assuming Voigt peak shapes. The fat peaks included were methyl at 0.90 parts per million (ppm), methylene at 1.30 ppm, β-carboxyl at 1.60 ppm, α-olefinic at 2.02 ppm, and α-carboxyl at 2.24 ppm, diallylic methylene at 2.75 ppm, glycerol at 4.20 ppm, and olefinic at 5.29 ppm.[23] Water signal was not detectable due to the strong diffusion-weighting. Only the methylene peak area (at 1.3 ppm) was used for further analysis because of the large peak area. ADC was determined by an exponential fitting of the methylene peak area as a function of *b*-value.

3.2 | Laser interferometer setup

To quantify the scanner table vibrations during the MR measurements, the displacements of the scanner table were measured by utilizing laser doppler interferometry (PSV-500-3D-Xtra, Polytec GmbH, Waldbronn, Germany). The interferometer setup was placed within the scanner room with a sufficient distance from the MR scanner such that the local magnetic field did not exceed 1 mT. The interferometer used infrared light with a wavelength of 1550 nm and a specific power of $P < 10$ mW. This way, it was possible to measure the table surface as well as the relative structural vibrations of the phantoms surface. With the setup at hand, a measurement sensitivity of 0.1 μm/s of the surface velocity could be realized. A schematic setup is shown in Figure 3.

3.3 | Laser interferometer measurements

Three different phantoms were utilized in the phantom measurements. For the lipid diffusion property measurements, 2 WF phantoms with 80% fat fraction were produced (content: 800 mL sunflower oil, 200 mL water, 4 mL Tween80, and 1 g of sodium benzoate). Emulsification was carried out with a colloid mill at 6000 and 11,000 revolutions per minute (rpm). The obtained phantoms yield different lipid droplet sizes and consequently different viscosities. However, the content of the WF phantoms was fluid. For the interferometer measurement reflective spray had to be attached to the phantom surface, and the experiment had to be performed with an open lid to directly measure on the phantom material. Therefore, the experiments with the laser interferometer were performed with an agar phantom (4% agar) that consisted of a solid material. All MR phantom experiments were performed with a 3 Tesla scanner (Ingenia Elition, Philips, Best) using an 8-channel wrist coil with the following common sequence parameters: Volume of Interest = $(15\ mm)^3$, TE = 60 ms, TM = 300 ms, TR = 1800 ms. The experiments were performed on the scanner table and on a decoupling table made of wood (Figure 3B) that decoupled the sample from the vibrating scanner table. The following 2 interferometer experiments were performed with the interferometer setup to quantify the effects under investigation.

First, the agar phantom was placed on the scanner table, and a high *b*-value DW MRS experiment with a *b*-value of

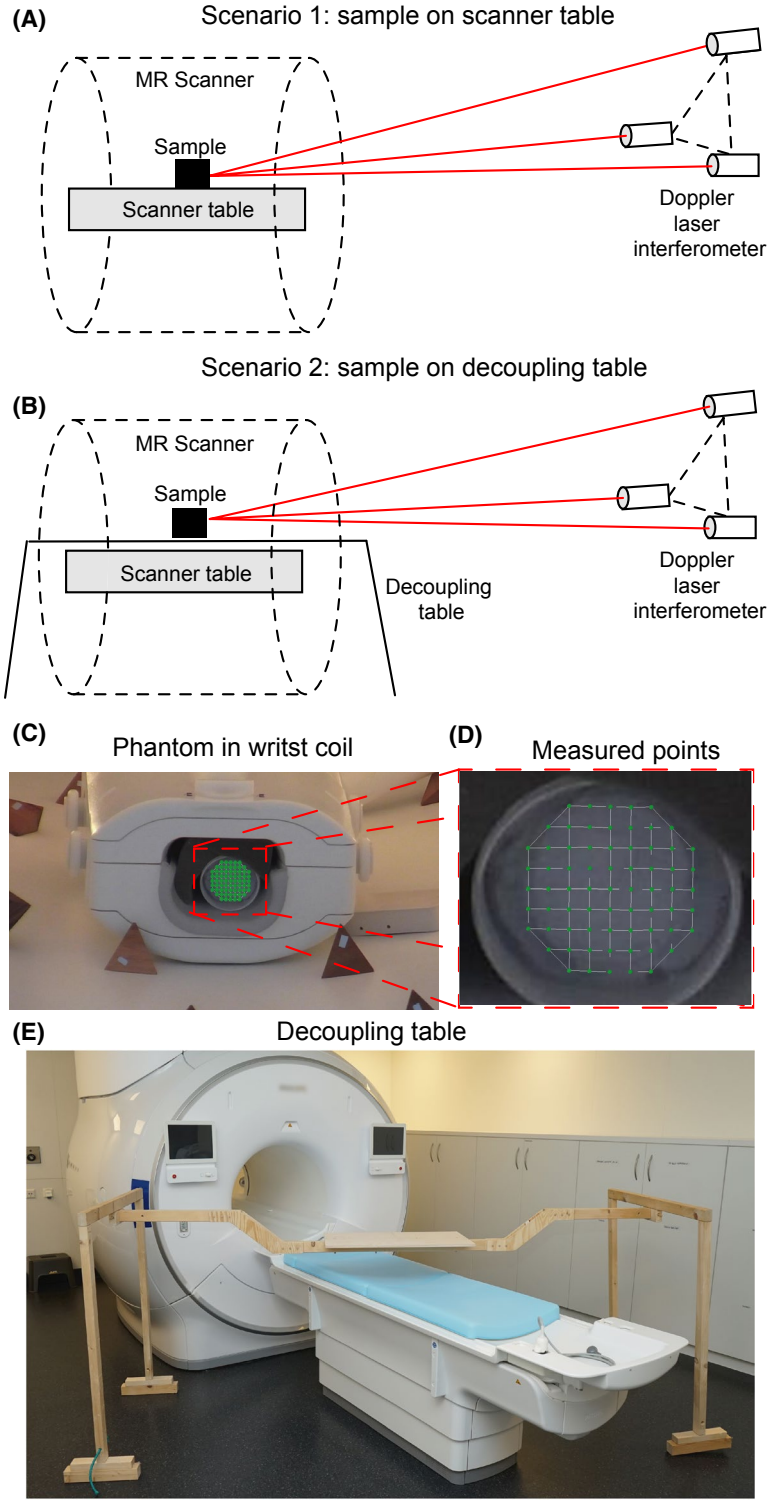

FIGURE 3 Experimental setup of the doppler laser interferometer measurement. 2 measurement scenarios can be distinguished: In the first scenario, the sample was measured directly on the scanner table (plot A). In the second scenario, the sample was placed on a decoupling table (plot B). The 3D displacement on the surface of a phantom was measured simultaneously from 3 doppler laser interferometers during the MR experiment to disentangle the displacements in all 3 spatial components. Plot C shows the measured agar phantom in the wrist coil, and plot D shows a zoom-in picture on the points that were measured on the top of the phantom surface. When only 1 spatial point was measured, the measurement point was placed in the middle of the surface. Plot E shows the decoupling wooden table

50,000 s/mm^2 was performed while varying the timing of the VMG from 50 ms to 650 ms in 5 ms steps.

Next, the laser was placed on a point in the middle of the phantom surface (Figure 3D), and the displacements in all 3 dimensions were acquired with 2 averages per timing. The 2 averages were combined, and the displacements during both diffusion gradients were extracted for each timing of the VMG. As a next step, the total accumulated phase was calculated based on Equation 3. The experiment was repeated with the 6000 rpm WF phantom without measuring displacements using the laser interferometer, and the methylene peak amplitude was extracted for different timings of the VMG.

Second, the timing of the VMG relative to DG_1 was set to match the diffusion time, and the displacements were acquired on the whole 2D surface of the agar phantom (70 measurement points) to investigate the phase dispersion

on a 2D surface. The experiment was repeated for 3 different measurement scenarios: without VMG and coil placed on the scanner table, with VMG and coil placed on scanner table, and without VMG and coil placed on the decoupling table. The accumulated phase was then calculated for each point, and the total signal within the 2D surface was calculated similar to Equation 5:

$$S = \sum_{n=1}^{N} e^{-i\phi_n}. \quad (7)$$

Here, N is the number of total measurement points (measurement points on the edge were excluded to avoid measurement artifacts due to the coupling to the probe holder). The signal on the scanner table was compared relative to the signal acquired on the decoupling table.

3.4 | ADC measurements in phantoms

To evaluate the performance of the proposed scheme, the lipid ADC value was estimated within the WF phantoms (6000 and 11,000 rpm). The voxel of interest was placed in the middle of the WF phantom material. The experiment was repeated for the same 3 different measurement scenarios as performed in the interferometer measurements and with the same scanning parameters. The utilized additional sequence parameters were: 16 averages per *b*-value (half of the averages with positive and the other half with negative polarity), 1 startup cycle, *b*-values = 10,000 – 20,000 – 40,000 – 60,000 s/mm^2, 2:48 min scan time per phantom. Diffusion gradients were applied simultaneously in all 3 axes to minimize TE.

3.5 | ADC measurements in vivo

The bone marrow in the tibia of 3 healthy volunteers (volunteer 1: 24 years/85 kg; volunteer 2: 29 years/57 kg; volunteer 3: 28 years/80 kg) was scanned using an 8-channel extremity coil without and with the VMG and with different additional weight placed on the scanner table (0/10/20 kg). By changing the loading of the scanner table, the mechanical vibrations were altered, and the influence of the vibrations on the DW measurement could be investigated. Each scan was repeated 3 times to access the reproducibility of the ADC measurement. The DW MRS voxel was placed approximately 1 cm below the growth plate in the tibia bone marrow and was performed with the same parameters as the phantom scans (including the same diffusion directions and *b*-values). Afterwards, the lipid ADC was extracted for each loading without and with the VMG.

4 | RESULTS

4.1 | Mechanical modeling of a 2-mass-spring-damper system

Figure 2 shows the results of the modeling of the mechanical system when actuated by the gradient pulse sequence depicted in the Figure 2A. The amplitude of the displacements during DG_1 are smaller compared to the displacements during DG_2 for both masses without the VMG. In addition, the shape of the displacements is different during both diffusion gradient durations when no VMG is employed, resulting in an additional phase accumulation when a magnetic field gradient is employed in the direction of the displacement. The amount of accumulated phase is thus different for both masses because the displacement curves also differ in their appearance without the VMG. With the VMG, the simulated displacement curves during both diffusion gradient durations and for both simulated masses are very similar. Such a phase accumulation pattern would result in a negligible phase difference between the 2 masses, inferring a minimal intramass dephasing when the phase of the 2 masses is combined.

4.2 | Quantification of scanner table vibrations by laser interferometry

Figure 4 shows the measured displacements on the agar phantom for 3 different measurement scenarios: without VMG on the scanner table, with VMG on the scanner table, and without VMG on the decoupling table. In general, the displacement in *z*-direction (feet-head) is small in all 3 measurements compared to the other components. In *x*-direction (right-left), minor deviations in the displacement can be seen in all 3 measurement scenarios. In *y*-direction (anterior-posterior), the displacements show an offset during the first and second diffusion gradient duration when the phantoms are placed on the scanner without the VMG, whereas the displacement patterns during the 2 diffusion gradients are very similar when the VMG is additionally employed. On the decoupling table, the displacements patterns are very similar and small for all components and show a very low- and very high-frequency component compared to the 20 to 25 Hz vibration visible on the results on the scanner table.

In Figure 5, the pulse sequence with the corresponding displacements during both diffusion gradients (DG_1 and DG_2) can be seen for 3 different timings of the VMG. Visually, a great difference in the displacement patterns can be seen when the timing of the additional gradient is much smaller or much larger than the diffusion time. Large differences in the displacements during the diffusion weighting gradients lead to accumulated phase that is not rephased and can lead

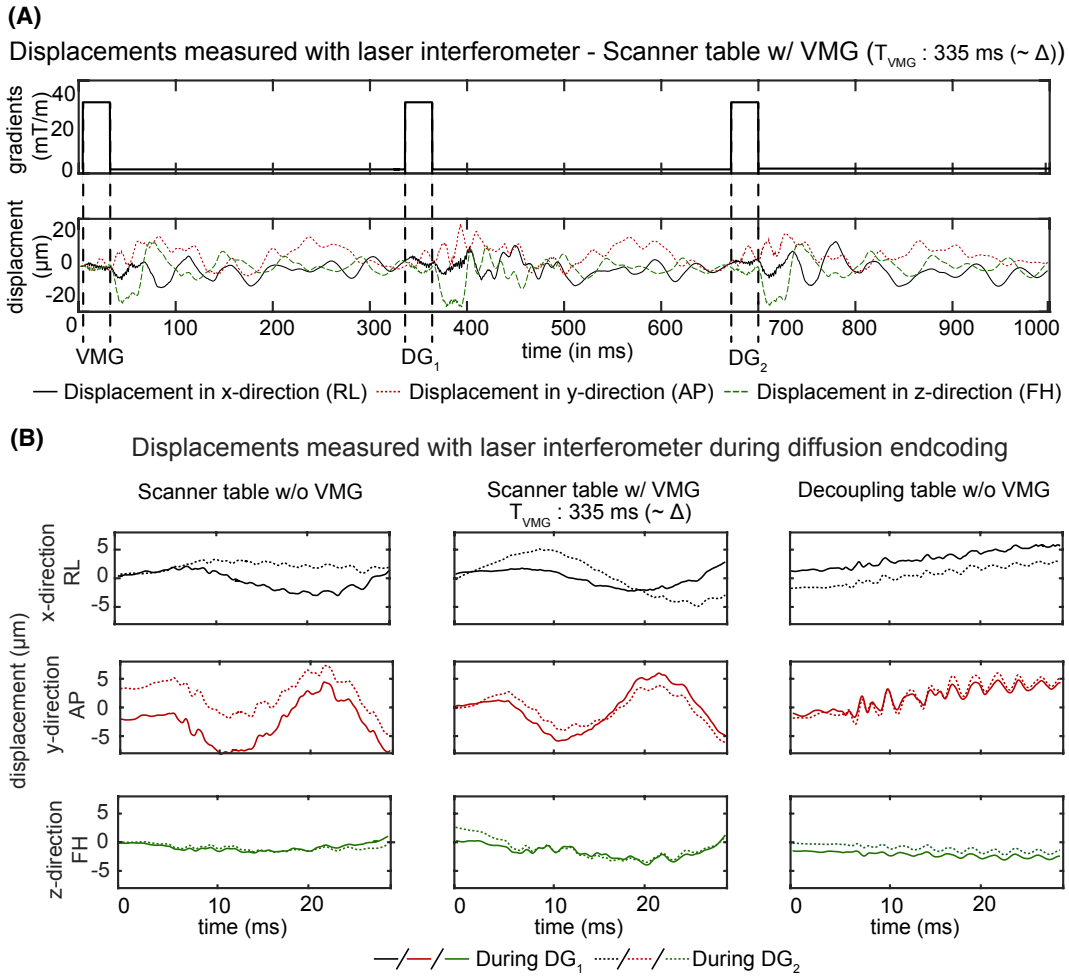

FIGURE 4 Measured displacements with laser interferometry when the T_{VMG} matched the diffusion time (Δ) (subplot A). Subplot B shows the *x*, *y*, and z displacements during DG_1 and DG_2 for 3 different measurement scenarios (different rows). Without the VMG, large differences between the displacement patterns can be seen compared to the case with the VMG (especially in *y* direction). Displacements are also visible with the decoupling table but follow the same patterns during both diffusion gradients

to signal loss. When the timing of the VMG is similar to the diffusion time, the displacement curves are similar.

Based on the displacement curves and the employed gradients, the phase difference for each VMG timing can be calculated based on Equation 4. Figure 6 shows the additional accumulated phase by vibrational displacements and compares it to the methylene peak amplitude acquired in a separate scan with the WF phantom. In general, areas with high and low accumulated phase can be observed with a similar pattern as the methylene peak area. When the diffusion time matches the VMG timing, a maximum in signal amplitude with corresponding minimum in the accumulated phase can be observed.

Figure 7 shows the accumulated phase that was calculated for a 2D surface on the agar phantom for different scenarios of phantom placement.

When the phantom is placed on the scanner table without the VMG, the accumulated phase during the diffusion weighting gradient has larger variations when compared to the scenario with the VMG. This results in a relative signal of 95% on the scanner table without the VMG compared to the signal on the decoupling table without the VMG. A relative signal of 99% on the scanner table with the VMG compared to the signal on the decoupling table without the VMG is observed.

4.3 | Lipid ADC measurements in phantoms

Figure 8 shows the results from the phantom scans. Assuming that the phantoms on the decoupling table are not affected by vibration artifacts, the ADC value on the decoupling table represents the real lipid ADC value. In the 6000 rpm phantom, the DW MRS experiment on the scanner table yields to a 119.0% overestimation of the ADC value, whereas only a relative error of 5.5% is observed on the scanner table with the VMG. In the 11,000 rpm phantom, the obtained lipid ADC value is very similar between the different

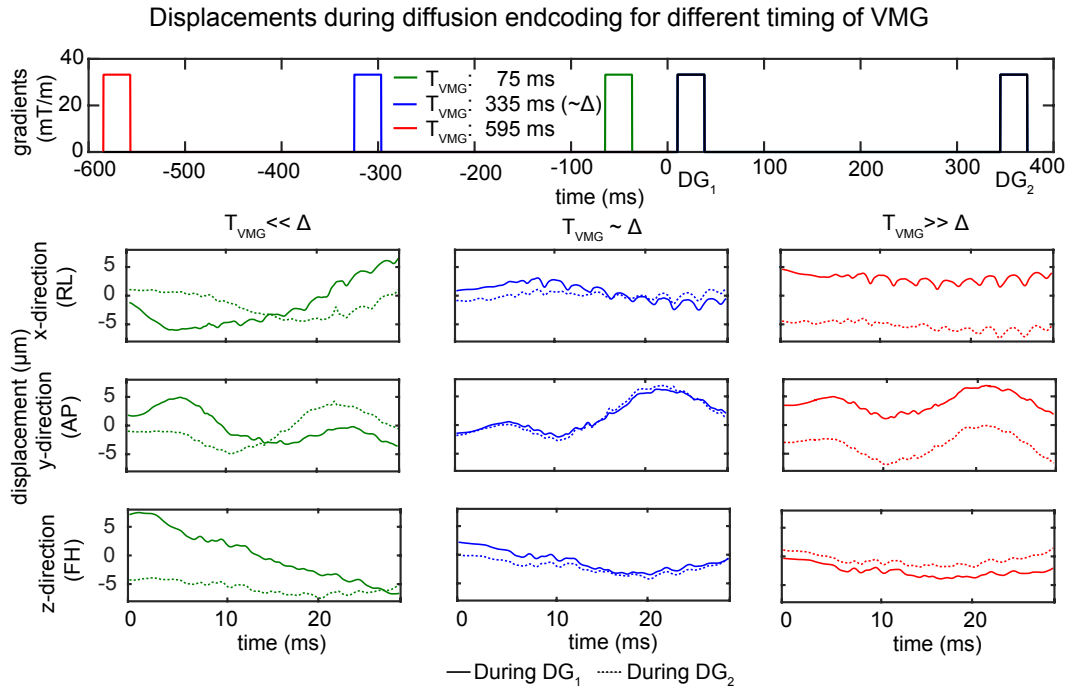

FIGURE 5 Measured *x*, *y*, and *z* displacements with laser interferometry during DG_1 and DG_2 for 3 different timings of the VMG. The first row shows the corresponding gradient pulse sequence. When the T_{VMG} is much smaller or larger than Δ, large variations of the displacements can be observed. When the T_{VMG} is equal to Δ, the displacement patterns are very similar

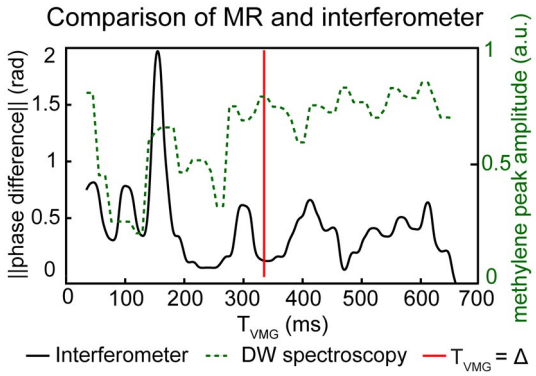

FIGURE 6 Accumulated phase on single point based on displacements measured with laser interferometry on the phantom surface (solid line) and methylene peak area acquired by DW-MRS for different T_{VMG} is shown. A maximum in signal amplitude corresponds to a minimum of acquired phase when T_{VMG} is equal to the Δ. Multiple minima of the phase and maxima of the methylene peak area can be observed

measurement scenarios, and only relative differences below 1% are observed.

4.4 | Lipid ADC measurements in vivo

Figure 9 shows the mean obtained ADC value in the tibia bone marrow, with corresponding SD of the 3 repeated measurements with different loading of the scanner table. Without the VMG, a dependency of the measured ADC value on the additional loading of the scanner table is observed, and a larger SD of the lipid ADC estimation is observed. The ADC value combined from the different measurement is comparable with and without VMG. However, the coefficient of variation is reduced by 34.9% (volunteer 1), 18.9% (volunteer 2), and 24.0% (volunteer 3) in the 3 volunteers, comparing the measurement without the VMG to the measurement with the VMG.

5 | DISCUSSION

The present study investigates the influence of mechanical vibrations on the signal of DW-MR measurements, focusing on the example of a high *b*-value DW MRS sequence and proposing a method to mitigate the signal loss by the application of an additional gradient. The main underlying concept does not eliminate mechanical vibrations but aims to approximately match the vibrational states during both diffusion gradients so that the total intravoxel dephasing is small and will not lead to significant signal loss.

The simplified mechanical system used to illustrate the transfer of vibrations within the tissue does by no means fully represent the complexity of soft tissue viscoelastic mechanics. Due to the adopted simplifications and the absence of accurate values for the mechanical properties, no quantitative analysis was performed, and only qualitative results were

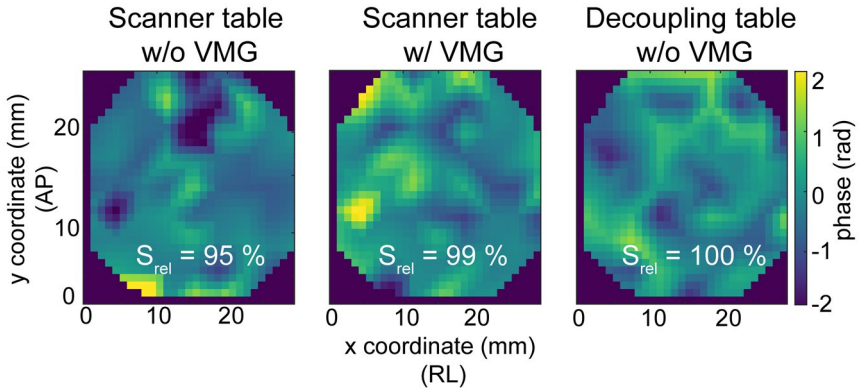

FIGURE 7 Accumulated phase on a 2D surface measured with laser interferometry on top of an agar phantom for 3 different scenarios. (A) phantom placed on the scanner table without VMG, (B) phantom placed on the scanner table with VMG, and (C) phantom placed on the decoupling table without VMG. When the phantom is solely placed on the scanner table, a 5% decay of the total signal can be observed in the measured 2D surface. When the phantoms are placed on the scanner table with the VMG, only a 1% decay of the signal is observed. It is expected that the signal decay will be larger when displacements over a 3D volume instead of over a 2D surface are measured

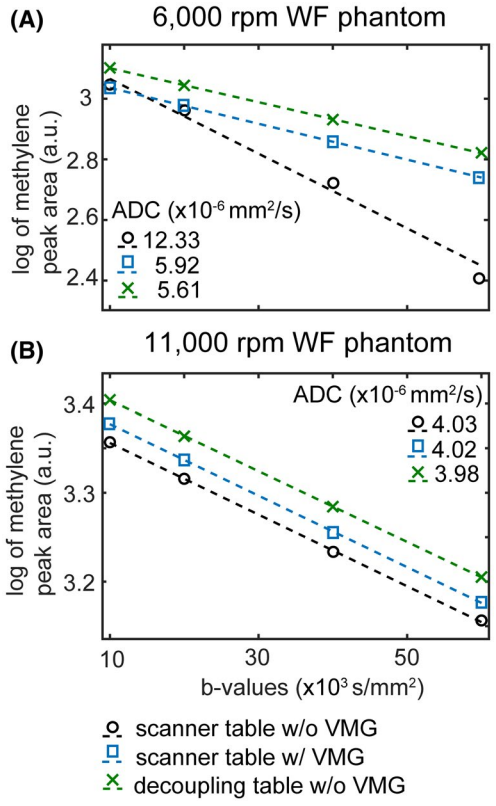

FIGURE 8 ADC determination in 6000 rpm (A) and the 11,000 rpm (B) water–fat (WF) phantoms. In the 6000 rpm phantom, a large difference in the lipid ADC value was observed without the VMG compared to the other 2 measurement scenarios. In the 11,000 rpm phantom, the differences between the measured lipid ADC values were minor. WF, water–fat

shown. The model reveals that the application of the VMG before the actual diffusion-weighting helps to approximately match the displacement patterns during both diffusion gradient durations. This is true for the investigated first mass that is directly excited by the impulse and also for the second mass that is connected to the first mass. When applying the VMG, both masses show a very similar displacement pattern during the diffusion encoding gradients, which would result in a very small accumulated phase during diffusion weighting. When the displacement pattern is different during the 2 diffusion gradients (as in the simulated case without the VMG), phase is accumulated. When this accumulated phase also varies for different positions within the tissue, the phase dispersion would result in signal losses within a voxel. Figure 2 clearly shows this variation of displacement patterns during the 2 diffusion gradient durations for the 2 simulated masses when no VMG is employed.

In Figure 4A, the measured displacements with VMG and T_{VMG} equal to the diffusion time in a real experimental setting are shown. The displacement pattern is similar but more complex than shown in the simplified model (Figure 2A). In Figure 4B, the displacements during the 2 diffusion gradients are depicted. The displacements differ when the phantom is measured on the scanner without applying the VMG and become more similar when the VMG is applied before the DW. This effect is especially prominent in the *y*-direction (anterior-posterior), whereas the *x*-direction (right-left) seems to be less affected by the application of the additional gradient. In *z*-direction (feet-head) the measured displacements are small compared to the other directions.

Displacements are also visible during the diffusion gradient durations when the coil is placed on the decoupling table. However, the displacements when the coil is placed on the decoupling table seem to be very similar during the diffusion gradients and represent much lower frequencies of the system. The decoupling table was manufactured with wood, which could result in low eigenfrequencies of the system. However, high vibrational frequency components can also be observed in anterior-posterior direction. This could potentially reflect

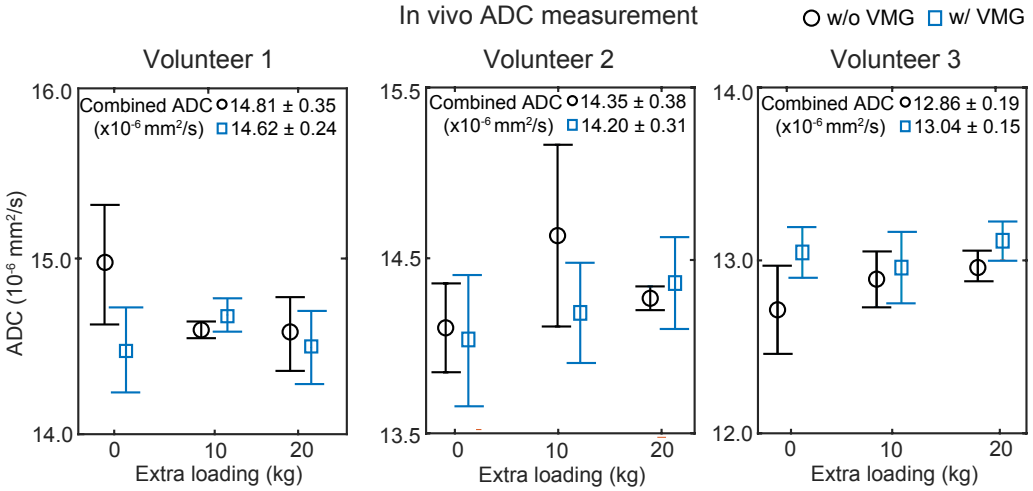

FIGURE 9 In vivo lipid ADC measurement in the tibia bone marrow for different loadings (0–10–20 kg additional weighting) on the scanner table in 3 healthy volunteers. Without the VMG, the measured ADC is dependent on the extra loading of the scanner table, and a larger ADC SD is observed. When all measurements are combined, the coefficient of variation is reduced by 34.9% (volunteer 1), 18.9% (volunteer 2), and 24.0% (volunteer 3) comparing the measurement without the VMG to the measurement with the VMG

the first natural resonance of the wooden decoupling table that is predominately present in anterior-posterior direction. The energy to excite this natural resonance vibration could also be transferred from the gradient coil to the decoupling table via sound waves.

Not only the employment of the VMG is important but also the timing of this additional gradient. Figure 5 shows that the displacement patterns differ greatly (even more compared to the absence of the VMG) when the VMG timing is much shorter or longer than the diffusion time. When the VMG replicates the shape and strength of the DW gradients and the timing of the diffusion preparation, the similarity of the displacement curves is very high.

Based on the measured displacements, the accumulated phase can be estimated and compared to the signal amplitude of a DW MRS scan. The results shown in Figure 6 represent a merging of 2 experiments, which could not be performed simultaneously. Therefore, although the location of the minima in the accumulated phase and maxima in the methylene peak area do not fully match, the pattern in the 2 curves of Figure 6 appears similar. Figure 6 shows that a maximum in the signal amplitude is obtained when the VMG timing relative to DG_1 is equal to the diffusion time. This high signal value corresponds to a minimum in the accumulated phase. The above finding is another illustration of the idea that the signal loss in a DW MR experiment due to vibrational artifacts can be reduced when the displacements during the 2 diffusion gradients are similar and eventually the accumulated phase is small. Figure 6 shows multiple minima in the accumulated phase or maxima in the signal values. However, the occurrence of these extreme values is not easily predictable without the knowledge of the exact mechanical properties of the system. Nevertheless, it can be postulated without any knowledge of the object properties that a minimum in the accumulated phase occurs when the VMG timing relative to the first diffusion gradient is equal to the diffusion time.

Solely accumulated phase is not sufficient to induce signal loss by intravoxel dephasing. For this effect, a phase dispersion over the 3D voxel needs to be present. To quantify the phase dispersion for more than 1 point, the accumulated phase was calculated on a 2D surface on top of the phantom. The surfaces shown in Figure 7 represent the accumulated phase in each point for different measurement scenarios. Signal loss will occur in DW MR experiments when a large spatial variation of phase is present in 1 acquisition voxel. The phase variation in a 2D surface can already give a hint to the expected signal loss in a 3D volume. When the phantom was scanned on the scanner table without the proposed scheme, a signal loss of 5% already could be observed in the 2D surface, whereas it was only 1% when the VMG was employed. It would be expected that the signal loss in a 3D volume on the scanner table will be higher without the VMG compared to the case with the VMG.

The phantom results in the 2 measured WF phantoms need to be discussed separately: In the 6000 rpm WF phantom, the lipid ADC value is greatly overestimated when the phantom is measured on the scanner table without the proposed method. When the VMG is employed, a great improvement in the measurement of the lipid ADC value can be observed. In the 11,000 rpm WF phantom, the ADC measurement seems to not be affected a lot by vibrations; therefore, the 3 measurement scenarios give very similar lipid ADC values. The differences in both phantoms can be explained by different oil droplet sizes within the 2 phantoms,[12] resulting in different viscoelastic properties of the phantoms: the 11,000 rpm phantom is more viscous than the 6000 rpm

phantom. Therefore, the effect of the vibrations on the overall signal loss is highly dependent on the tissue properties and can vary a lot between different tissue type. However, it should be noted that the VMG does not cause artifacts in the ADC quantification when the estimation without the additional gradient is already sufficient (as can be seen in the 11,000 rpm WF phantom). Therefore, the application of the VMG overall improves the accuracy of the measured lipid ADC value in phantoms.

The coefficient of variation for the estimation of in vivo lipid ADC decreased significantly when the VMG was employed in all 3 volunteers. A correct estimation of the diffusion properties of lipids is particularly important when high order effects such as diffusion restriction effects are investigated.[12] The ADC value changes in an 80-μm diameter fat cell in vivo by approximately 1% per 100 ms diffusion time increase.

Therefore, a high accuracy in the DW signal acquisition is needed. The presented method could be used to improve the quality of DW MR measurements and eventually the accuracy of lipid droplet size estimations.

The proposed study has the following limitations: First, the laser interferometer data and the DW-MRS data were acquired subsequently and not in the same phantom. However, experimental limitations did not allow a simultaneous acquisition in the same phantoms. Consequently, the slight mismatch between the accumulated phase curve and the methylene peak amplitude in Figure 6 could most likely be explained by the different phantom materials with different viscoelastic effects. This difference in the material properties leads to differences in the observed displacement with different frequencies and damping. However, the overall trend is also visible in this merged dataset based on different experiments. Second, the phase dispersion was only measured on a 2D surface and not in a 3D volume. For an accurate estimation of the intravoxel dephasing effect with the corresponding signal loss, the accumulated phase should be calculated for each point in a 3D volume. However, the employed laser interferometer methodology only allows measurements on a surface without depth information. Because phase dispersion effects are even visible on a 2D surface, phase dispersion effects are expected to be present and may be even more severe if the measurements would have been extended to a 3D analysis. The presented measurements do not allow for an accurate quantification of the 3D intravoxel phase dispersion; however, based on the 2D surface information, conclusions can be drawn that the signal loss should be reduced when the VMG is applied.

Another way of reducing vibrational artifacts in diffusion-weighted sequences would be the reduction of acoustic noise produced by the applied gradients. This could be achieved by either matching the frequency of the time-varying diffusion gradient to minima of the scanner gradient response function[24] or by reducing the slew rate of the diffusion gradients. However, the above approaches would lead to less flexibility in the selection of sequence timing and most probably to prelonged TEs.

The proposed approach can be theoretically applied in other DW MR sequences with minor or negligible time penalty by adding the VMG before the start of the diffusion preparation.

An even better matching of the vibrational states might be achieved by extending the VMG and also adding additional other gradients (e.g., slice selection gradients or spoiler gradients) in the gradient prepulse. The proposed approach could be also of interest in DW imaging of the brain, where vibration induced artifacts were reported previously.[7] Especially in pediatric cases, vibration effects could be even more severe due to the light weight of the patients and the typical optimization of the scanner hardware toward adult weights and dimensions.[8] The general trend toward high *b*-value brain diffusion that allows high-resolution diffusion tensor imaging with fiber tracking comes with the cost of stronger and longer diffusion gradients.[9] Such more demanding requirements on the gradient scanner hardware are expected to increase the occurrence and strength of vibration artifacts. The proposed VMG is not able to completely recover the lost signal but can reduce the artifact with minor penalty on the acquisition time. Further studies should focus on the application of the proposed technique on other DW measurements to reduce artifacts.

6 | CONCLUSION

A method was proposed to mitigate signal loss in DW measurements induced by scanner table vibrations. The benefit for placing an additional gradient before the DW module in a DW MRS sequence was shown by mechanical modeling and by measuring the actual displacements on the surface of a phantom during a DW MRS measurement. When using the additional gradient, the displacements during the diffusion gradients were more similar, which would result in less signal loss by intravoxel dephasing. The application of the proposed method showed an improvement in lipid ADC quantification in WF phantoms and in the tibia bone marrow of 3 healthy volunteers.

ACKNOWLEDGMENTS

We would like to thank the company Polytec GmbH for their support in performing the laser interferometer measurements. We would also like to thank Dr. Rainer Burgkart for help in the construction of the decoupling table and Dr. Curtis Johnson for valuable discussions. We would also like to thank Julius Honecker and Oliver Gmach for their help constructing the water-fat phantoms. The present work was supported

by the European Research Council (grant agreement 677661, ProFatMRI). This work reflects only the authors' view, and the European Research Council is not responsible for any use that may be made of the information it contains. In addition, the authors acknowledge research support from Philips Healthcare.

ORCID

Dominik Weidlich https://orcid.org/0000-0001-7842-2682
Marcus Maeder https://orcid.org/0000-0001-8541-8630
Stefan Ruschke https://orcid.org/0000-0001-9658-6541
Dimitrios C. Karampinos https://orcid.org/0000-0003-4922-3662

REFERENCES

1. Jones DK. *Diffusion MRI: Theory, Methods, and Applications*. New York, NY: Oxford University Press; 2012.
2. Anderson AW, Gore JC. Analysis and correction of motion artifacts in diffusion weighted imaging. *Magn Reson Med*. 1994;32:379–387.
3. Reese TG, Heid O, Weisskoff RM, Wedeen VJ. Reduction of eddy-current-induced distortion in diffusion MRI using a twice-refocused spin echo. *Magn Reson Med*. 2003;49:177–182.
4. Steidle G, Eibofner F, Schick F. Quantitative diffusion imaging of adipose tissue in the human lower leg at 1.5 T. *Magn Reson Med*. 2011;65:1119–1125.
5. Hiltunen J, Hari R, Jousmaki V, Muller K, Sepponen R, Joensuu R. Quantification of mechanical vibration during diffusion tensor imaging at 3 T. *NeuroImage*. 2006;32:93–103.
6. Gallichan D, Robson MD, Bartsch A, Miller KL. TREMR: table-resonance elastography with MR. *Magn Reson Med*. 2009; 62:815–821.
7. Gallichan D, Scholz J, Bartsch A, Behrens TE, Robson MD, Miller KL. Addressing a systematic vibration artifact in diffusion-weighted MRI. *Hum Brain Mapp*. 2010;31:193–202.
8. Berl MM, Walker L, Modi P, et al. Investigation of vibration-induced artifact in clinical diffusion-weighted imaging of pediatric subjects. *Hum Brain Mapp*. 2015;36:4745–4757.
9. Setsompop K, Kimmlingen R, Eberlein E, et al. Pushing the limits of in vivo diffusion MRI for the Human Connectome Project. *NeuroImage*. 2013;80:220–233.
10. Cao P, Fan S-J, Wang AM, et al. Diffusion magnetic resonance monitors intramyocellular lipid droplet size in vivo. *Magn Reson Med*. 2015;73:59–69.
11. Verma SK, Nagashima K, Yaligar J, et al. Differentiating brown and white adipose tissues by high-resolution diffusion NMR spectroscopy. *J Lipid Res*. 2017;58:289–298.
12. Weidlich D, Honecker J, Gmach O, et al. Measuring large lipid droplet sizes by probing restricted lipid diffusion effects with diffusion-weighted MRS at 3T. *Magn Reson Med*. 2019;81:3427–3439.
13. Lehnert A, Machann J, Helms G, Claussen CD, Schick F. Diffusion characteristics of large molecules assessed by proton MRS on a whole-body MR system. *Magn Reson Imaging*. 2004;22:39–46.
14. Suzuki M, Shinohara Y, Ohsaki Y, Fujimoto T. Lipid droplets: size matters. *J Electron Microsc (Tokyo)*. 2011;60(suppl 1):S101–S116.
15. Cousin B, Cinti S, Morroni M, et al. Occurrence of brown adipocytes in rat white adipose tissue: molecular and morphological characterization. *J Cell Sci*. 1992;103:931–942.
16. Scheller EL, Doucette CR, Learman BS, et al. Region-specific variation in the properties of skeletal adipocytes reveals regulated and constitutive marrow adipose tissues. *Nat Commun*. 2015;6:7808.
17. Callaghan PT. *Principles of Nuclear Magnetic Resonance Microscopy*. Oxford University Press on Demand; 1993.
18. Hurwitz R, Lane SR, Bell RA, Brant-Zawadzki MN. Acoustic analysis of gradient-coil noise in MR imaging. *Radiology*. 1989; 173:545–548.
19. Stejskal EO, Tanner JE. Spin diffusion measurements: spin echoes in the presence of a time-dependent field gradient. *J Chem Phys*. 1965;42:288–292.
20. Low G, Kruse SA, Lomas DJ. General review of magnetic resonance elastography. *World J Radiol*. 2016;8:59–72.
21. Gao L, Parker KJ, Lerner RM, Levinson SF. Imaging of the elastic properties of tissue—a review. *Ultrasound Med Biol*. 1996; 22:959–977.
22. Vöth S. *Dynamik schwingungsfähiger Systeme: Von Der Modellbildung bis zur Betriebsfestigkeitsrechnung mit MATLAB/SIMULINK*. Wiesbaden, Germany: Vieweg+Teubner Verlag; 2007.
23. Ruschke S, Kienberger H, Baum T, et al. Diffusion-weighted stimulated echo acquisition mode (DW-STEAM) MR spectroscopy to measure fat unsaturation in regions with low proton-density fat fraction. *Magn Reson Med*. 2016;75:32–41.
24. Schmitter S, Diesch E, Amann M, Kroll A, Moayer M, Schad LR. Silent echo-planar imaging for auditory FMRI. *MAGMA*. 2008;21:317–325.

SUPPORTING INFORMATION

Additional supporting information may be found online in the Supporting Information section.
Equations of motion for 2 mass-spring-damper system

How to cite this article: Weidlich D, Zamskiy M, Maeder M, Ruschke S, Marburg S, Karampinos DC. Reduction of vibration-induced signal loss by matching mechanical vibrational states: Application in high *b*-value diffusion-weighted MRS. *Magn Reson Med*. 2020;84:39–51. https://doi.org/10.1002/mrm.28128